

SCIENTIFIC REPORTS



OPEN

Combined study of the ground and excited states in the transformation of nanodiamonds into carbon onions by electron energy-loss spectroscopy

Zhenbao Feng¹, Yangming Lin², Cunwei Tian¹, Haiquan Hu¹ & Dangsheng Su³

The electron momentum density and sp^2/sp^3 ratio of carbon materials in the thermal transformation of detonation nanodiamonds (ND) into carbon nano-onions are systematically studied by electron energy-loss spectroscopy (EELS). Electron energy-loss near-edge structures of the carbon K-ionization in the electron energy-loss spectroscopy are measured to determine the sp^2 content of the ND-derived samples. We use the method developed by Titantah and Lamoen, which is based on the ability to isolate the π^* spectrum and has been shown to give reliable and accurate results. Compton profiles (CPs) of the ND-derived carbon materials are obtained by performing EELS on the electron Compton scattering region. The amplitude of the CPs at zero momentum increases with increasing annealing temperature above 500 °C. The dramatic changes occur in the temperature range of 900–1300 °C, which indicates that the graphitization process mainly occurs in this annealing temperature region. Our results complement the previous work on the thermal transformation of ND-derived carbon onions and provide deeper insight into the evolution of the electronic properties in the graphitization process.

Nanodiamonds (NDs) and carbon nano-onions (CNOs), currently attract enormous attention and exhibit promising perspectives in applications. Nanodiamonds are excellent candidates as metal-free catalysts, drug delivery vectors and biomedical markers^{1–4}. Potential applications of carbon onions include solid lubrication, anode materials for Li-ion batteries, electromagnetic shielding, metal-free catalysts, fuel cells and electrochemical energy storage^{1,5–7}. At present, annealing nanodiamonds in an inert atmosphere or in vacuum is the most effective way to produce carbon onions^{5,8}. The phase transform process includes nanodiamonds, bucky-diamond and carbon onions, which correspond to the sp^3 -bonded, mixed sp^2/sp^3 -bonded and sp^2 -bonded carbon atoms, respectively. In the course of this transformation, the carbon hybridization changes from sp^3 to sp^2 and occurs from the surface inward. Raman spectroscopy, high-resolution transmission electron microscopy (HRTEM) and X-ray photoelectron spectroscopy (XPS) have been used to study this transformation under successive annealing treatments^{8–10}. It is found that (i) annealing of nanodiamonds in an inert environment leads to the sp^3 -to- sp^2 conversion beginning at the surface of smaller nanodiamonds at temperatures of 600–700 °C; (ii) annealing temperatures above 1000 °C, the majority of detonation nanodiamonds are partially or fully converted to carbon onions depending on the crystal size; (iii) an almost total completion of the transformation after annealing occurs at temperatures greater than 1500 °C. However, most of these studies have focused on the morphological and structural changes of annealing nanodiamonds during successive annealing temperatures. Until now, the full electronic structures of annealing nanodiamonds during the graphitization process of this sp^3 -to- sp^2 conversion remains poorly understood. The numerous potential applications of nanodiamonds and carbon onions make it both scientifically interesting and technologically important to study the electronic properties during the phase transformation.

¹School of Physical Science and Information Technology, Shandong Key Laboratory of Optical Communication Science and Technology, Liaocheng University, 252059, Liaocheng, China. ²Max-Planck Institute for Chemical Energy Conversion, 45470, Mülheim, Germany. ³Dalian National Laboratory for Clean Energy, Dalian Institute of Chemical Physics, Chinese Academy of Sciences, 116023, Dalian, China. Correspondence and requests for materials should be addressed to Z.F. (email: fengzhenbao@lcu.edu.cn)

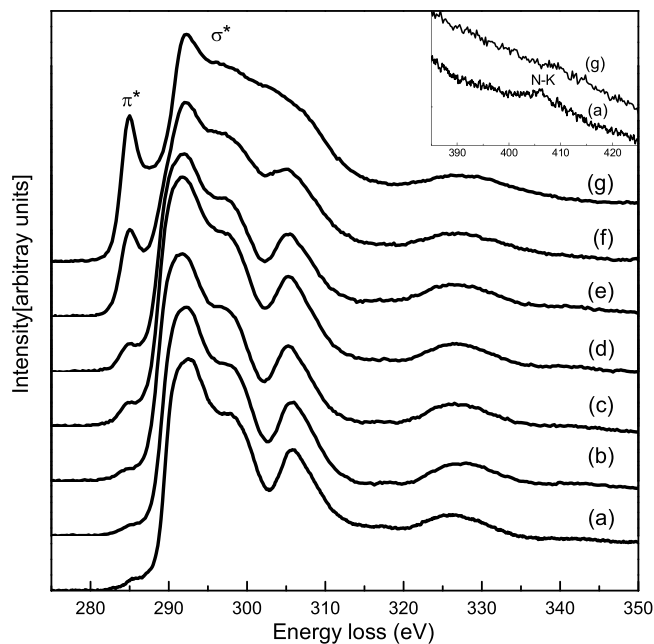


Figure 1. Experimental carbon K-edge fine structure (ELNES) spectra of (a) ND, (b) ND500, (c) ND700, (d) ND900, (e) ND1100, (f) ND1300 and (g) ND1500. The inset shows the region of nitrogen K-edge.

With the popularization of transmission electron microscopy (TEM) in laboratories, electron energy-loss spectroscopy (EELS) has become a standard analytical technique to determine the chemical composition, bonding information, optical properties and electronic structure of solids^{11–13}. The low-loss region of EELS reflects the dielectric response of the material. The most commonly-used region of EELS, termed the electron energy-loss near-edge structure (ELNES), reflects the unoccupied density of states as well as the transition-matrix element¹⁴. Therefore, the information extracted from this region relates to the excited state electronic structure, bonding as well as orbital hybridization of the specimen. The Compton profile can be extracted from EELS in the large energy-loss region (more than 1000 eV), known as the electron Compton scattering from solids (ECOSS)¹⁵. In terms of electron microscopy, ECOSS is electron energy-loss spectrum (EELS) recording in diffraction mode at large scattering angle, performing an energy scan across the Bethe ridge^{16–18}. ECOSS is a powerful tool to study the ground-state electronic momentum density of solids, especially for nanomaterials^{17,19}. Recently, ECOSS measurements can be achieved in 1 minute for one available Compton profile^{20–22}. The short recording time makes it practicable to study the Compton profile as a function of temperature, composition or orientation of the material²³.

EELS has been used to study nanodiamonds and carbon onions^{10,24}, where the spectra show typical diamond-like (sp^3) and graphite-like (sp^2) energy-loss near-edge structures, respectively. We have performed an initial study of the sp^2 content with increasing temperature through measuring ELNES of annealing nanodiamonds based on the three-Gaussian (TG) method²⁴. For the TG method, a small change of the energy upper limit for the fitting or the location of the second peak leads to a significant fluctuation of the sp^2 fractions^{25,26}. There is still much uncertainty of the sp^2 fractions determined by the TG method for the nanodiamonds-to-carbon onions conversion.

In this work, we employ electron energy-loss spectroscopy to monitor both the sp^2 -bonded carbon fractions and the ground-state electronic momentum density distributions in the transformation of nanodiamonds into carbon onions with increasing the annealing temperatures. Through recording ELNES of ND-derived samples in the thermal transformation, the sp^2 percentages were determined by the method developed by Titantah and Lamoen, which has been shown to give relatively accurate results²⁵. A series of electron energy-loss spectra of samples in the transformation were measured in the Compton scattering regions. Valence Compton profiles of each carbon material in the transformation of nanodiamonds into carbon onions were obtained by ECOSS analysis.

Results and Discussion

Sp^2/sp^3 ratio. Figure 1 shows ELNES of the C-K edge from a series of ND-derived samples at different annealing temperatures after a power-law type background subtraction. We focused on two main typical peaks for the carbon materials in EELS, π^* and σ^* peaks. The π^* peak was located at approximately 285 eV, which was associated to the excitations of the 1s core level electrons to unoccupied anti-bonding π^* states for sp^2 -hybridized carbon atoms. The sharp peak σ^* at approximately 292 eV arose from transitions of the 1s core level electrons to unoccupied anti-bonding σ^* states. These two main features were observed in Fig. 1 for all spectra. With increasing temperatures, the relative intensity of the π^* peak increased. The rate of increase was negligible before the annealing temperature of 900 °C. This indicated the sp^2 -hybridized carbon atoms didn't undergo pronounced

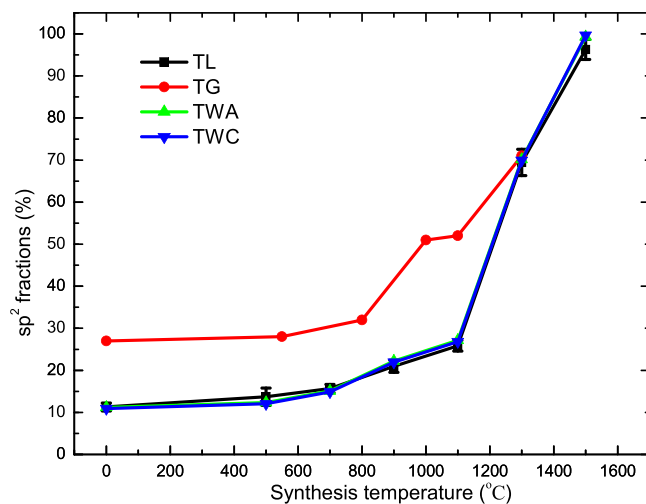


Figure 2. sp^2 fractions of ND-derived samples in the thermal transformation of nanodiamonds to carbon onions by TL method (black) along with results obtained from the TG (red)²⁴, TWA (green) and TWC (blue) methods. The error bars (black) are plotted for our TL results.

increase before the annealing temperature of 900 °C. This was consistent with the onset of graphitization for ND when approaching 800–900 °C^{8,27}. As shown in the inset, a clear signal for the nitrogen K-edge was present at 406 eV for the ND sample. Nitrogen is commonly found in detonation NDs synthesized with nitrogen-containing explosives^{2,5}. The peak of the nitrogen K-edge disappeared for the ND1500 sample (carbon onions). The nitrogen dopants were lost in the process of reconstructive phase transformation from sp^3 -hybridized diamond to sp^2 -hybridized carbon onions^{6,27}. No oxygen signal (K-edge of oxygen at 532 eV) was detected in these investigated samples.

The transformation of nanodiamonds into carbon onions involves sp^3 -bonded carbon atoms becoming sp^2 -bonded carbon atoms. The intermediate phase of carbon, named “bucky diamond”, with a nanodiamond core is covered by an onion-like carbon outer shell. Bucky diamond is formed by the mixed sp^2/sp^3 bonding of carbon atoms. The optical, electrical, mechanical and thermal properties of carbon materials are known to be particularly relevant to the bonding states of carbon atoms in a material. The sp^2/sp^3 ratio of carbon materials can be determined by several techniques, such as X-ray photoelectron spectroscopy, Raman spectroscopy, X-ray absorption near-edge spectroscopy and electron energy-loss near-edge spectroscopy^{24,28,29}. Among them, electron energy-loss near-edge structure in combination with transmission electron microscopy is now the most powerful technique to quantify the ratio of sp^2/sp^3 -hybridized carbons. The intensity of I_{π^*} only stems from the contributions of carbons with sp^2 -hybridization. Both sp^3 - and sp^2 -hybridized carbons show strong contributions to the intensity of I_{σ^*} . The appearance of the π^* peak can be used as a sign of sp^2 -hybridized carbons. Thus, the hybridization ratio of the studied samples can be determined by applying Eq. (1)

$$sp^2 = \frac{[I_{\pi^*}/I_{total}]_{sample}}{[I_{\pi^*}/I_{total}]_{100\% sp^2 reference, HOPG}} \quad (1)$$

The ratio is zero for purely sp^3 -hybridized carbons (diamond) and 100% for purely sp^2 -hybridized carbons (highly ordered pyrolytic graphite, HOPG). To avoid the possible influence of anisotropy on the samples, all ELNES measurements should be carried out at the magic-angle condition. Several approaches have been suggested and have discussed how to determine I_{π^*} and I_{total} , for example, “two-window method” with windows aligned on the edge onset (TWA), “two-window method” with windows centrally positioned to the major peaks (TWC), three-Gaussian (TG) methods and other model fitting methods^{25,26,29}. Bernier *et al.* have reviewed these methods and discussed the advantages and disadvantages for each of them²⁶. TWA, TWC and TG methods ignore the contributions in σ^* region for the I_{π^*} calculation. In this work, we applied the Titantah and Lamoen (TL) method to determine the fraction of sp^2 -hybridized carbons during transformation from ND to CNO. This sp^3/sp^2 characterization technique is based on the ability to isolate the π^* features, independent of the position of the π^* and σ^* peak, the size of the energy window and the fewest fitting parameters. Figure 2 shows our calculated sp^2 fractions using TL along with TG methods²⁴. The TG method gives higher sp^2 fractions during the transformation, especially at a low annealing temperature. Below 900 °C, the TG method showed that the sp^2 fractions approached 30%, while no more than 20% was obtained for the TL method. Numerous studies have shown that sp^3 to sp^2 conversion mainly occurs on the surface of ND powders without altering the diamond core below 900 °C in an inert atmosphere. The sp^2 fractions are attributed to a thin layer of amorphous and disordered carbon on the surface of ND or the surface reconstructs into graphitization at low annealing temperature. It can be noted that the sp^2 fraction dramatically increased above 1100 °C for the TL results. This is consistent with results from Raman spectroscopy and TEM analysis⁸. For comparison, we also calculated the sp^2 fractions by TWA and TWC methods. The results are consistent with that of TL method, as shown in Fig. 2.

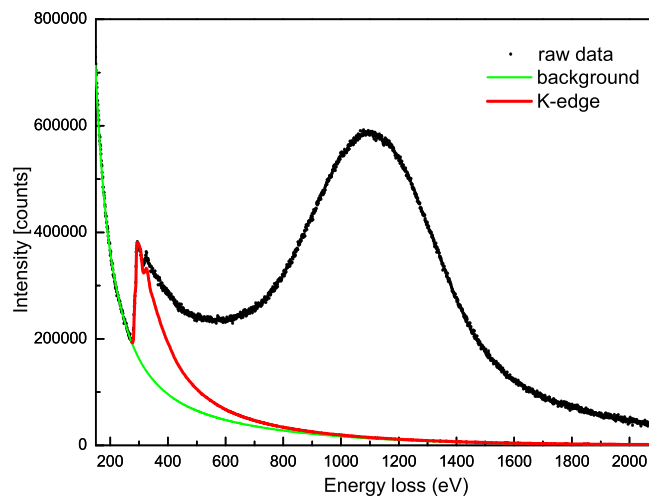


Figure 3. Raw EELS data of ND1500 (carbon onions) for ECOS analysis along with the simulated background by parameterized elastic-inelastic scattering events and the contributions of the carbon K-ionization edge.

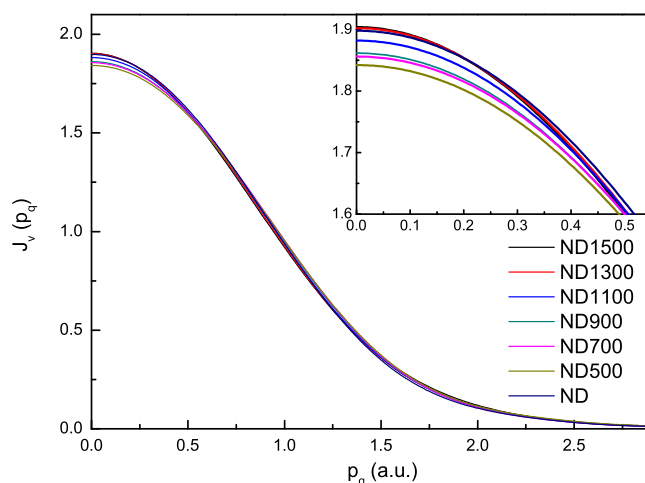


Figure 4. Valence Compton profiles of ND, ND500, ND700, ND900, ND1100, ND1300 and ND1500 (CNOs).

Electron momentum density. As a representation, the raw ECOS data of ND1500, recorded by electron energy-loss spectroscopy, are shown in Fig. 3. The background was determined by parameterizing simulations of the combined elastic and inelastic scattering. The total exposure time was 2 min for each spectrum. This short recording time provided us with an opportunity to systematically study the electron momentum distributions of the transformation from ND to CNOs with annealing temperature. Figure 4 shows valence Compton profiles (CP) of ND, ND500, ND700, ND900, ND1100, ND1300 and ND1500. Details of the experimental and analytical procedures have been presented previously^{19,20}. The amplitude of CPs increased with an increase of the annealing temperature above 500 °C. The amplitude of CP for ND500 was smaller than that of ND at zero momentum. This indicated a higher localization of the electron density distribution for ND in momentum space or higher delocalization in real space. Using Raman spectroscopy, the thermal transformation of nanodiamonds to carbon onions has been shown to start at 600 °C upon annealing in an argon atmosphere. Chemically, the raw detonation ND consists of 80–90% of the carbon in the mass, a few mass% of oxygen, hydrogen, nitrogen, and minor amounts of other impurities⁵. Oxygen and hydrogen emerge in the form of surface functional groups. The transformation is a multistep process. In general, the transformation starts with desorption of water and detachment of oxygen-containing surface functional groups on the surface of ND when heated up to approximately 200 °C. Increasing the temperature will remove functional groups like carboxyl, anhydride and lactone groups. Further increasing the temperature leads to the sp^3 -to- sp^2 conversion from the surface inward. The functional groups and disordered carbon on the surface of ND are associated with the greater delocalization of the ground state charge density in real space.

The differences between the profiles of ND700, ND900, ND1100, ND1300 and ND1500 with respect to ND500 are shown in Fig. 5. The evolution process of CPs for the transformation of “pure” sp^3 -hybridized diamond to sp^2 -hybridized carbon onions is clearly shown. The amplitude of CPs increased with respect to that of

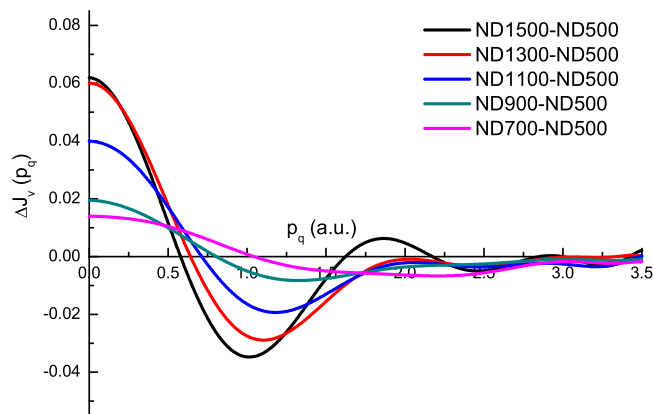


Figure 5. Profiles of ND700, ND900, ND1100, ND1300 and ND1500 with respect to ND500.

ND500. At $p_q = 0$, the ND1500 (carbon onions) profile was higher by 3% than that of ND500. This indicated a greater delocalization of the valence electrons in real space in the carbon onions. It should be mentioned that the density of nanodiamonds (3.3 g/cm^3) was much higher than that of carbon onions ($\sim 1.9 \text{ g/cm}^3$). The decrease of density in the transformation from nanodiamonds to carbon onions induces an increase in the particle volume. The volume expansion is expected to generate a larger delocalization of the charge density in carbon onions. In addition, we found the dramatic changes of CPs occur in the range of 900–1300 °C. We thus conclude that the majority of the sp^3 -to- sp^2 conversion occurs in this temperature region. This conclusion is consistent with our ELNES study and previous work using other techniques^{8,27}.

Conclusions

Both the unoccupied and ground-state electronic properties of ND-derived carbon materials in the thermal transformation from ND to CNOs have been systematically studied by electron energy-loss spectroscopy using a transmission electron microscope. Electron energy-loss near-edge spectra of the carbon K-ionization were recorded at the optical axis to study the evolution of unoccupied states in the transformation. The sp^2 fractions were determined by the TL method, which has been shown to give reliable and accurate results. Compared with the TG method, the TL method gives a lower sp^2 content for ND-derived carbon materials at an annealing temperature below 1100 °C. Electron energy-loss spectra of a series of ND-derived carbon materials were recorded at large scattering angles (around 73 mrad) with short exposure time. The valence Compton profiles in the transformation were obtained by ECOSS analysis. Compared with “pure” NDs, the CPs of carbon onions indicated a substantially greater delocalization of the ground-state charge density. Investigation of both sp^2 fractions and Compton profiles indicated the majority of sp^3 -to- sp^2 conversion occurred at the thermal annealing temperatures of 900–1300 °C. This conclusion is consistent with previous works that used other techniques. ECOSS is shown to be a sensitive probe of the binding structure in nanomaterials. The short recording time enables the study of Compton profiles as a function of temperature. The ECOSS technique will be a powerful tool to study the ground-state electron momentum density distribution of a system and is highly sensitive to the change of ground-state wave functions, especially for carbon nanomaterials.

Methods

Electron energy-loss near-edge structure. The quantity measured in an EELS experiment is the double differential scattering cross section (DDSCS). In the first-order Born approximation, the DDSCS for fast electrons is given by¹⁶.

$$\frac{\partial^2 \sigma}{\partial E \partial \Omega} = \frac{4\gamma^2 k_1}{a_0^2 q^4 k_0} S(\mathbf{q}, E) \quad (2)$$

here a_0 is the Bohr radius, γ is the relativistic factor, and k, k_0 are wavevectors of the fast electron before and after scattering. $\hbar\mathbf{q} = \hbar(\mathbf{k}_0 - \mathbf{k}_1)$ is the momentum transfer in the scattering process. The dynamic structure factor $S(\mathbf{q}, E)$, a function of the momentum transfer \mathbf{q} and energy loss E , is given by

$$S(\mathbf{q}, E) = \sum_{i,f} |\langle i | e^{i\mathbf{q}\cdot\mathbf{r}} | f \rangle|^2 \delta(E + E_i - E_f) \quad (3)$$

here $|f\rangle$ and $|i\rangle$ are the final and initial states of the atoms, with energies E_f and E_i , respectively, and \mathbf{r} is the position operator. The sum is over all occupied initial and unoccupied final states.

The physical information of the DDSCS depends on the regime of the momentum transfer \mathbf{q} and energy loss E in the dynamic structure factor [DFF]. To explain the near-edge structure in the EELS spectrum, the DFF following from band structure calculations can be rewritten as:

$$S(\mathbf{q}, E) = \left| \int \psi_i e^{i\mathbf{q}\cdot\mathbf{r}} \psi_f^* d^3\mathbf{r} \right|^2 \rho(E) \quad (4)$$

In Eq. (4), ψ_i and ψ_f are the initial and final state wave functions, respectively. $\rho(E)$ is the density of the final (or unoccupied) states (DOS). In this expression, the DFF is divided into two parts: the transition-matrix elements and the DOS term $\rho(E)$. The transition-matrix term determines the basic edge shapes. For small momentum transfers ($\mathbf{q} \cdot \mathbf{r} \ll 1$), the operator reduces to a dipole approximation. The DOS term gives the fine structure on the basic near edge. Usually, the ELNES are recorded with the collection aperture centered on the optic axis in the TEM, and therefore, simply reflects the unoccupied density of states.

Electron Compton scattering from solids. Most of the EELS experiments are performed around the unscattered electrons. If we tilt the incident beam through a few degrees so that only large-angled scattering electrons are recorded, a broad peak emerges at the high energy loss region, which is known as the electron Compton scattering spectrum. If the energy transfer is much greater than the binding energy of the atomic electron and the momentum transfer in the scattering process is significantly large relative to the inverse electronic orbital size, the binary-encounter impulse approximation (IA) is valid. Under the IA condition, the DFF can be given as³⁰:

$$S(\mathbf{q}, E) = \frac{m}{\hbar q} J(p_q) \quad (5)$$

Here, p_q is the projection of the electron momentum along the direction of momentum transfer q and $J(p_q)$ is taken as the definition of the Compton profile

$$J(p_q) = 2\pi \int_{p_q}^{\infty} |\chi(p_i)|^2 p_i dp_i \quad (6)$$

where $\chi(p_i)$ is the momentum wave function of the initial state. Therefore, Compton profiles provide a direct experimental method to measure the ground state wave function of an electron in real space through the Fourier transform. The energy loss E in the IA condition is given by p_q as^{17,31}

$$E = E_{\max} + p_q (2E_{\max})^{1/2} \quad (7)$$

where E_{\max} is the energy loss of Compton peak (Eq. (7) is obtained when $m_e = c = \hbar = 1$). Eq. (7) is a critical step in the ECOSS analysis since it is used to convert the energy scale of a measured energy-loss spectrum to the momentum scale.

Experimental. Purified ultra-dispersed nanodiamonds (UDD) were purchased from Beijing Grish Hitech Co. (China), which were produced by detonation and purified by acid washing. The average size of UDD was ~5 nm. Noncombustible contaminations were determined by an inductively coupled plasma optical emission spectrometer, and included Al < 50 ppm, Cu < 10 ppm, Cr < 10 ppm, Ca < 50 ppm, Fe < 50 ppm, Mg < 10 ppm and Ti < 10 ppm. Samples ND500, ND700, ND900, ND1100, ND1300 and ND1500 (CNOs) were produced by annealing purified UDD at 500, 700, 900, 1100, 1300 and 1500 °C for 4 h in an argon atmosphere, respectively. Each TEM specimen was prepared by ultrasonic vibration in pure ethanol for 10 mins and then depositing a drop of the suspension onto a TEM holey carbon grid. We have done EELS studied on specimens suspended over holes in the carbon support grid. Experiments were carried out on a FEI Tecnai G2 F20 microscope equipped with a Gatan GIF 963 spectrometer at an accelerating voltage of 200 kV. ELNES of each sample was recorded at the magic angle condition (collection angle ~1.5 mrad) with the entrance aperture centered on the optic axis under the parallel incident beam^{32,33}. The energy resolutions were 0.8 eV (the full width at half maximum of the zero-loss peak, FWHM). For ECOSS acquisitions, thin regions with a diameter of approximately 800 nm were chosen by the convergent incident beam. The convergence angle was 3.5 mrad and the collection angle was 2.44 mrad. EELS spectra for ECOSS in the range of more than 2000 eV were recorded at a scattering angle of approximately 73 mrad. The Compton peak was located at approximately 1100 eV for each ECOSS measurements. The energy resolutions were 3 eV (FWHM) and the corresponding momentum resolution was 0.012 a.u. for the Compton profiles. Considering the recording conditions (beam convergence and collection angle), the total momentum resolutions were estimated to be in the order of 0.1 a.u.¹⁷. It is only possible to obtain such a good momentum resolution for photon Compton scattering by using a synchrotron radiation source. More than five measurements were taken at different positions for each sample to reduce the statistical error. The thickness or ELNES for each sample were measured before and after ECOSS measurements to make sure the sample had not suffered serious radiation damage.

References

1. Mochalin, V. N., Shenderova, O., Ho, D. & Gogotsi, Y. The properties and applications of nanodiamonds. *Nat. Nanotechnol.* **7**, 11–23 (2012).
2. Turner, S. *et al.* Aberration-corrected microscopy and spectroscopy analysis of pristine, nitrogen containing detonation nanodiamond. *Physica Status Solidi a-Applications and Materials Science* **210**, 1976–1984 (2013).
3. Nee, C. H., Yap, S. L., Tou, T. Y., Chang, H. C. & Yap, S. S. Direct synthesis of nanodiamonds by femtosecond laser irradiation of ethanol. *Sci Rep-Uk* **6**, 33966 (2016).
4. Pichot, V., Muller, O., Seve, A., Yvon, A. & Merlat, L. Optical properties of functionalized nanodiamonds. *Sci Rep-Uk* **7**, 14086 (2017).

5. Zeiger, M., Jackel, N., Mochalin, V. N. & Presser, V. Review: carbon onions for electrochemical energy storage. *J Mater Chem A* **4**, 3172–3196 (2016).
6. Zeiger, M., Jackel, N., Asian, M., Weingarth, D. & Presser, V. Understanding structure and porosity of nanodiamond-derived carbon onions. *Carbon* **84**, 584–598 (2015).
7. d'Amora, Marta *et al.* Biocompatibility and biodistribution of functionalized carbon nano-onions (f-CNOs) in a vertebrate model. *Sci Rep-Uk* **6**, 33923 (2016).
8. Cebik, J. *et al.* Raman spectroscopy study of the nanodiamond-to-carbon onion transformation. *Nanotechnology* **24**, 205703 (2013).
9. Suarez, S. *et al.* In-situ nanodiamond to carbon onion transformation in metal matrix composites. *Carbon* **129**, 631–636 (2018).
10. Mykhaylyk, O. O., Solonin, Y. M., Batchelder, D. N. & Brydson, R. Transformation of nanodiamond into carbon onions: A comparative study by high-resolution transmission electron microscopy, electron energy-loss spectroscopy, x-ray diffraction, small-angle x-ray scattering, and ultraviolet Raman spectroscopy. *J. Appl. Phys.* **97**, 074302 (2005).
11. Zhang, Z. L. *et al.* Investigating the structure of non-graphitising carbons using electron energy loss spectroscopy in the transmission electron microscope. *Carbon* **49**, 5049–5063 (2011).
12. Glasel, J. *et al.* Mesoporous and Graphitic Carbide-Derived Carbons as Selective and Stable Catalysts for the Dehydrogenation Reaction. *Chem. Mater.* **27**, 5719–5725 (2015).
13. Zhang, B. S. & Su, D. S. Transmission Electron Microscopy and the Science of Carbon Nanomaterials. *Small* **10**, 222–229 (2014).
14. Keast, V. J., Scott, A. J., Brydson, R., Williams, D. B. & Bruley, J. Electron energy-loss near-edge structure - a tool for the investigation of electronic structure on the nanometre scale. *J. Microsc.* **203**, 135–175 (2001).
15. Williams, B. G., Sparrow, T. G. & Egerton, R. F. Electron Compton scattering from solids. *Proc. R. Soc. Lond. A* **393**, 409–422 (1984).
16. Egerton, R. F. *Electron energy-loss spectroscopy in electron microscope*, Edn. Third. (Springer, New York 2011).
17. Jonas, P. & Schattschneider, P. The experimental conditions for Compton scattering in the electron microscope. *J. Phys.: Condens. Matter* **5**, 7173–7188 (1993).
18. Schattschneider, P. & Exner, A. Progress in electron Compton scattering. *Ultramicroscopy* **59**, 241–253 (1995).
19. Feng, Z. B. Doctoral Thesis (Vienna University of Technology, Vienna, 2013).
20. Feng, Z. B. *et al.* Combined study of the ground and unoccupied electronic states of graphite by electron energy-loss spectroscopy. *J. Appl. Phys.* **114**, 183716 (2013).
21. Feng, Z. B., Yang, B., Lin, Y. M. & Su, D. S. Communication: Investigation of the electron momentum density distribution of nanodiamonds by electron energy-loss spectroscopy. *J. Chem. Phys.* **143**, 211102 (2015).
22. Feng, Z. B., Sakurai, Y., Liu, J. F., Su, D. S. & Schattschneider, P. Anisotropy of electron Compton profiles of graphite investigated by electron energy-loss spectroscopy. *Appl. Phys. Lett.* **108**, 093108 (2016).
23. Cooper, M. J., Mijnders, P. E., Shiotani, N., Sakai, N. & Bansil A. X-Ray Compton scattering (Oxford University Press, New York, 2004).
24. Wang, R., Sun, X. Y., Zhang, B. S., Sun, X. Y. & Su, D. S. Hybrid nanocarbon as a catalyst for direct dehydrogenation of propane: formation of an active and selective core-shell sp²/sp³ nanocomposite structure. *Chem. Eur. J.* **20**, 6324–6331 (2014).
25. Titantah, J. T. & Lamoen, D. Technique for the sp²/sp³ characterization of carbon materials: Ab initio calculation of near-edge structure in electron-energy-loss spectra. *Phys. Rev. B* **70**, 075115 (2004).
26. Bernier, N. *et al.* A methodology to optimize the quantification of sp² carbon fraction from K edge EELS spectra. *J. Electron. Spectrosc. Relat. Phenom.* **164**, 34–43 (2008).
27. Petit, T., Arnault, J. C., Girard, H. A., Sennour, M. & Bergonzo, P. Early stages of surface graphitization on nanodiamond probed by x-ray photoelectron spectroscopy. *Phys. Rev. B* **84**, 233407 (2011).
28. Titantah, J. T. & Lamoen, D. sp²/sp³ characterization of carbon materials from first-principles calculations: X-ray photoelectron versus high energy electron energy-loss spectroscopy techniques. *Carbon* **43**, 1311–1316 (2005).
29. Papworth, A. J., Kiely, C. J., Burden, A. P., Silva, S. R. P. & Amaratunga, G. A. J. Electron-energy-loss spectroscopy characterization of the sp² bonding fraction within carbon thin films. *Phys. Rev. B* **62**, 12628–12631 (2000).
30. Williams, B. G. *Compton Scattering*. (McGraw-Hill, New York 1977).
31. Jonas, P. Doctoral Thesis (Vienna University of Technology, Vienna 1993).
32. Hebert, C., Schattschneider, P., Franco, H. & Jouffrey, B. ELNES at magic angle conditions. *Ultramicroscopy* **106**, 1139–1143 (2006).
33. Schattschneider, P., Hebert, C., Franco, H. & Jouffrey, B. Anisotropic relativistic cross sections for inelastic electron scattering, and the magic angle. *Phys. Rev. B* **72** (2005).

Acknowledgements

This work was supported by the National Natural Science Foundation of China (Grant No. 11504386), Natural Science Foundation of Shandong Province (Grant No. ZR2016FQ05) and the Initial Foundation for Doctor Program of Liaocheng University (Grant No. 318051613). We thank Liwen Bianji, Edanz Group China (www.liwenbianji.cn/ac), for editing the English text of a draft of this manuscript.

Author Contributions

Z.F. performed EELS experiments. Y.L. prepared samples. Z.F., C.T. and H.H. analyzed the data and made figures. Z.F. and D.S. wrote the paper. All authors commented on the manuscript.

Additional Information

Supplementary information accompanies this paper at <https://doi.org/10.1038/s41598-019-40529-2>.

Competing Interests: The authors declare no competing interests.

Publisher's note: Springer Nature remains neutral with regard to jurisdictional claims in published maps and institutional affiliations.



Open Access This article is licensed under a Creative Commons Attribution 4.0 International License, which permits use, sharing, adaptation, distribution and reproduction in any medium or format, as long as you give appropriate credit to the original author(s) and the source, provide a link to the Creative Commons license, and indicate if changes were made. The images or other third party material in this article are included in the article's Creative Commons license, unless indicated otherwise in a credit line to the material. If material is not included in the article's Creative Commons license and your intended use is not permitted by statutory regulation or exceeds the permitted use, you will need to obtain permission directly from the copyright holder. To view a copy of this license, visit <http://creativecommons.org/licenses/by/4.0/>.

© The Author(s) 2019